SCIENCE CHINA
Information Sciences

• RESEARCH PAPER •

November 2026, Vol. 69, Iss. 11, 210202:1–210202:16
https://doi.org/10.1007/s11432-026-5238-7

Special Topic: Intelligent Characterization and Modeling for Complex Systems

Evolutionary dynamics of nonlinear multiplayer snowdrift games on higher-order networks

Changwei HUANG[1], Meiling LONG[1], Liming ZHANG[2*],
Tina P. BENKO[3] & Matjaž PERC[3,4,5,6*]

[1]*Guangxi Key Laboratory of Multimedia Communications and Network Technology, School of Computer, Electronics and Information, Guangxi University, Nanning 530004, China*
[2]*Jiangsu Key Laboratory of Educational Intelligent Technology, School of Artificial Intelligence and Computer Science, Jiangsu Normal University, Xuzhou 221116, China*
[3]*Faculty of Natural Sciences and Mathematics, University of Maribor, Maribor 2000, Slovenia*
[4]*Community Healthcare Center Dr. Adolf Drolc Maribor, Maribor 2000, Slovenia*
[5]*Department of Physics, Kyung Hee University, Seoul 02447, Republic of Korea*
[6]*University College, Korea University, Seoul 02841, Republic of Korea*

Received 5 April 2026/Revised 8 October 2026/Accepted 23 October 2026/Published online 10 November 2026

Abstract Collective cooperation is the cornerstone of human societal prosperity and development. While higher-order networks can characterize the properties of group interactions that transcend pairwise ties, the majority of evolutionary game models built upon them are constrained by linear payoff assumptions. This simplification fails to account for the nonlinear synergistic effects that are fundamental to collective action in many real-world systems. To bridge this gap, we propose a nonlinear multiplayer snowdrift game model on simplicial complex networks, and quantitatively characterize the synergy intensity of cost-sharing in different group-size interactions via parameterized second-order (ε_2) and third-order (ε_3) nonlinear synergy factors. We find that stronger synergy raises the critical cost-benefit ratio (r^*) for the evolution of cooperation, thereby enabling cooperative strategies to prevail across a broader parameter range. Furthermore, we find that as synergy intensity increases, high-degree cooperative nodes leverage topological heterogeneity to amplify nonlinear synergy gains. This process facilitates the formation of stable local cooperative clusters centered on high-degree nodes, ultimately driving the nucleation and diffusion of cooperative behaviors throughout the network.

Keywords evolutionary game dynamics, higher-order networks, multiplayer snowdrift game, nonlinear synergy

Citation Huang C W, Long M L, Zhang L M, et al. Evolutionary dynamics of nonlinear multiplayer snowdrift games on higher-order networks. Sci China Inf Sci, 2026, 69(11): 210202, https://doi.org/10.1007/s11432-026-5238-7

1 Introduction

Cooperation is pivotal to the prosperity and development of human societies. From addressing public crises and organizing team collaboration to maintaining the stability of ecosystems, the success of collective action relies heavily on effective cooperation among individuals [1–4]. However, cooperative behavior appears to contradict individual rationality. Understanding how cooperation emerges and is sustained has thus long been a core research question in evolutionary game theory [5, 6].

Early studies on the evolution of cooperation primarily relied on traditional networks, which only captured pairwise interactions [7–12]. In the real world, however, cooperation is not limited to bilateral interactions but prevails more extensively in group interaction scenarios involving three or more agents [13–19], such as mutualistic symbiosis in ecosystems and collective action in social systems. Higher-order interactions can generate non-additive group effects that cannot be inferred from pairwise interactions alone. Existing studies have analyzed the evolutionary dynamics of multiplayer games in well-mixed and structured populations [20–25]. In a well-mixed population, Wei et al. [26] introduced collective reputation assessment into public goods games and found that moderately strict group assessment can sustain cooperation. On graphs, Peña et al. [27] showed that the effect of population structure on cooperation depends on network topology. More recently, Wang et al. [28] developed a unified framework for pairwise and group cooperation on heterogeneous weighted social networks, finding that degree-inverse weighted ties promote cooperation in both settings. Beyond studying group cooperation on conventional networks, researchers

* Corresponding author (email: lmzhang@jsnu.edu.cn, matjaz.perc@gmail.com)

© Science China Press 2026

have used hypergraphs [29–34] and simplicial complexes [35–39] to represent group interactions directly as higher-order ties. This structural shift has yielded significant insights into the evolution of cooperation. Chen et al. [40] reviewed cooperation dynamics on higher-order networks across public goods, prisoner's dilemma, and snowdrift games, discussing how group structure and evolutionary mechanisms affect cooperative outcomes. From a broader perspective, Battiston et al. [41] examined how higher-order interactions shape collective human behaviour, including cooperation and coordination. In specific model studies, Alvarez-Rodriguez et al. [42] established a public goods game (PGG) model on hypergraphs and analyzed the impacts of group size and network structural heterogeneity on the evolution of cooperation. Guo et al. [43] investigated the evolutionary dynamics of mixed games on simplicial complex networks and revealed that higher-order networks exert a significant influence on the evolution of cooperation. The general game-theoretic framework proposed by Civilini et al. [44] demonstrated that higher-order interactions can enable the persistence of cooperation in scenarios that would otherwise lead to complete defection in the prisoner's dilemma. Sheng et al. [45] constructed an analytical framework for strategy evolution applicable to arbitrary higher-order population structures, considering spatial heterogeneity and nonlinear payoffs. Through analytical methods and validations on empirical networks, they revealed that higher-order interactions promote the evolution of cooperation in networks with interconnected communities. Focusing on strategy updating, Wang and Yi [46] introduced a two-stage imitation process on weighted hypergraphs and showed that selecting a high-performing group before randomly choosing a member to imitate can promote cooperation in public goods games. Wang et al. [47] investigated cooperative evolution on temporal hypergraphs, demonstrated that time-varying higher-order interactions promote cooperation more effectively than static structures, and clarified that sparse connected components and moderate hyperedge sizes can further enhance the emergence and persistence of cooperation. In addition, the effects of cooperation-promoting mechanisms such as reinforcement learning [48,49], reputation mechanisms [50,51], and structural heterogeneity [52–54] on higher-order networks have also been extensively investigated. Related studies have also explored voluntary participation and institutional incentive mechanisms in the evolution of cooperation. Shen et al. [55] found that exit options can sustain altruistic punishment in networked populations, and Chai et al. [56] employed the mean-field approximation to investigate the optimal tax–subsidy incentive for promoting cooperation.

Despite this progress, a critical simplification persists within most higher-order models: the assumption of linear payoffs, which stands in stark contrast to the inherently nonlinear effects of real-world group interactions [57–60]. For instance, in the collective hunting of African wild dogs, synergies from pack coordination cause per-capita costs to drop precipitously—far more rapidly than a linear function. Similarly, in large-scale engineering projects, specialization and resource sharing lead to a nonlinear decrease in the marginal cost for each participant. Research on nonlinear games began to address this, with Hauert et al. [61] notably being the first to introduce synergy effects and discount effects into public goods games. Zhu et al. [62] further constructed a probabilistic model where synergy and discount effects coexist stochastically. Jiang et al. [63] developed a co-evolutionary framework where the game environment itself is dynamically shaped by the collective behavior of the population, creating a closed-loop feedback between strategies and their payoff landscape. While these studies confirmed that nonlinear mechanisms better capture the complexity of group interactions, this line of inquiry has remained overwhelmingly focused on the PGG framework. In contrast, the multiplayer snowdrift game (MSG) [64–66], with its intrinsic cost-sharing mechanism, offers a more natural framework for studying such synergies. However, while preliminary work has applied the MSG to simplicial complexes [67], it retained a simplistic linear cost-sharing rule, focusing instead on other factors like the proportion of higher-order interactions. How parameterized synergy factors alter cost sharing and cooperative evolution in multiplayer snowdrift games on simplicial complexes therefore remains insufficiently understood.

To address these issues, this paper constructs a nonlinear multiplayer snowdrift game model on simplicial complex networks. We characterize the synergy level of cost-sharing across groups of varying sizes by introducing second-order and third-order nonlinear synergy factors. The evolutionary process follows the death-birth update rule, with the fixation probability serving as a metric for the level of cooperation. Through extensive Monte Carlo simulations, we systematically explore the interplay between these synergy factors, the cost-benefit ratio, and network topology on the evolution of cooperation. Furthermore, we examine local cooperation around high-degree nodes, the growth of cooperative clusters, and how the initial cooperator's degree relates to fixation probability. Finally, we test whether the main trends persist on simplicial complex networks generated by preferential attachment and on four empirical higher-order networks.

The main contributions of this study are as follows.

(1) A multiplayer snowdrift game model with a nonlinear cost-sharing rule is constructed on simplicial complex networks. In contrast to existing nonlinear public goods games, which place nonlinearity in the collective benefit, the proposed rule captures synergy through the cost borne by each cooperator, thereby extending earlier higher-order

snowdrift games beyond equal cost sharing. By introducing order-specific synergy factors ε_2 and ε_3, we characterize how the individual cost of cooperators varies with the number of cooperators in edge-based two-player and triangle-based three-player games, respectively. Our results demonstrate that increasing either factor elevates the critical cost-benefit ratio r^*, which allows cooperation to be favored by natural selection across a wider parameter space.

(2) The key role of high-degree nodes in the spread of cooperation is elucidated. We find that high-degree nodes are more capable of sustaining their own cooperative behavior throughout the evolutionary process, and this advantage becomes more pronounced as nonlinear synergy intensifies. By participating in more group interactions, high-degree cooperators accumulate a greater payoff advantage from synergistic cost sharing, which induces their neighbors to cooperate and fosters the formation of local cooperative clusters centered on them, ultimately promoting the spread of cooperation across the network.

(3) The robustness of these findings is verified on simplicial complexes generated by preferential attachment and on multiple real-world higher-order networks, where increasing the nonlinear synergy factors consistently facilitates the evolution of cooperation.

The rest of this paper is organized as follows. Section 2 introduces the model framework, including the construction of simplicial complex networks, the rules of the nonlinear snowdrift game, and evolutionary dynamics. Section 3 presents the results of simulation experiments and verifies the robustness of the conclusions on real-world network datasets. Section 4 summarizes the paper and outlines future research directions.

2 Models

2.1 Higher-order network construction

We model the population's interaction structure using a simplicial complex, a mathematical framework well-suited for representing higher-order interactions. A q-simplex, the fundamental building block of a simplicial complex, is a set of $q+1$ fully interconnected nodes representing a group interaction among $q+1$ agents. For example, a 0-simplex is a node, a 1-simplex is an edge (a pairwise interaction), and a 2-simplex is a triangle (a three-body interaction). In this work, we focus on a simplicial complex comprising a set of nodes $V = \{1, 2, \ldots, N\}$, a set of edges $E = \{e_1, e_2, \ldots, e_m\}$, and a set of triangles $T = \{\tau_1, \tau_2, \ldots, \tau_l\}$.

To generate networks with a rich higher-order structure, we employ a triangle growth algorithm inspired by [68,69]. While the original framework includes both random and preferential attachment, we utilize the random attachment variant. A key property of this method is that every new node introduced during the growth phase is immediately embedded within a 2-simplex, ensuring a pervasive triangular structure throughout the network. In this study, the network size is set to $N = 100$, and the initial number of network nodes is $N_0 = 5$. The detailed construction steps are as follows.

Step 1. Initialization. At the initial time step $t = 0$, we generate an initial network consisting of an N_0-clique (a complete graph where all N_0 nodes are connected to each other).

Step 2. Network growth. At each subsequent time step, a new node v_x is added to the current network. An existing edge $e = (v_i, v_j)$ is selected uniformly at random from the current edge set E. The new node v_x is then connected to both v_i and v_j, forming two new edges, (v_x, v_i) and (v_x, v_j). This process simultaneously creates a new 2-simplex (triangle), $\tau = (v_i, v_j, v_x)$.

Step 3. Iteration. Step 2 is repeated until the network reaches the desired size N.

2.2 Nonlinear multiplayer snowdrift game

In our model, individuals participate in multiplayer snowdrift games within local interaction groups defined by the network's simplices. The MSG captures the inherent tension between cooperation and free-riding in a collective action problem. In any given game played by a group of G individuals, each participant can either cooperate (C) to help complete a task or defect (D). The task, if completed, yields a benefit b to all G members, regardless of their strategy. The baseline cost of completing the task is c, which is also the cost borne by a lone cooperator, with $b > c > 0$.

2.2.1 *Linear cost-sharing baseline*

We first define the canonical MSG with a linear cost-sharing rule, which serves as a baseline for our model. In this standard setup, the cost c is divided equally among the n_C cooperators. Defectors, by definition, incur no cost. The

task is successfully completed if at least one individual cooperates ($n_C \geqslant 1$). The payoffs for a cooperator ($\bar{\Pi}_C$) and a defector ($\bar{\Pi}_D$) are thus given by

$$\begin{aligned} \bar{\Pi}_C(n_C) &= b - \frac{c}{n_C}, \quad \text{for } n_C \in \{1, \ldots, G\}, \\ \bar{\Pi}_D(n_C) &= \begin{cases} 0, & \text{for } n_C = 0, \\ b, & \text{for } n_C \in \{1, \ldots, G-1\}. \end{cases} \end{aligned} \tag{1}$$

To simplify the analysis, we normalize the payoffs by the benefit b, using the cost-benefit ratio $r = c/b$ [70]. The normalized payoffs are

$$\begin{aligned} \Pi_C(n_C) &= 1 - \frac{r}{n_C}, \quad \text{for } n_C \in \{1, \ldots, G\}, \\ \Pi_D(n_C) &= \begin{cases} 0, & \text{for } n_C = 0, \\ 1, & \text{for } n_C \in \{1, \ldots, G-1\}. \end{cases} \end{aligned} \tag{2}$$

Within our simplicial complex, the group size G is determined by the order of the interaction: $G = 2$ for pairwise interactions on 1-simplices (edges), and $G = 3$ for three-body interactions on 2-simplices (triangles).

2.2.2 *Nonlinear synergistic cost-sharing*

The linear cost-sharing rule in (2) fails to capture the nonlinear synergies often present in real-world cooperation, where per-capita costs can decrease much more rapidly as more individuals contribute. To model this phenomenon, we introduce parameterized synergy factors that modify the effective number of cost-sharers.

Specifically, we define a synergistic cost-sharing function $S(n_C, \varepsilon_m)$ that replaces the linear term n_C in the denominator of the cost expression as

$$S(n_C, \varepsilon_m) = 1 + \varepsilon_m + \varepsilon_m^2 + \cdots + \varepsilon_m^{n_C - 1}, \quad \text{for } n_C \geqslant 1, \tag{3}$$

where $\varepsilon_m \geqslant 0$ is an order-specific factor governing how the cost borne by each cooperator depends on the number of cooperators. The resulting cost per cooperator is

$$c_1(n_C, \varepsilon_m) = \frac{c}{S(n_C, \varepsilon_m)} = \frac{c}{1 + \varepsilon_m + \varepsilon_m^2 + \cdots + \varepsilon_m^{n_C - 1}}. \tag{4}$$

When $\varepsilon_m = 1$, $S(n_C, 1) = n_C$, and the model recovers conventional equal cost sharing. For $n_C \geqslant 2$, $0 \leqslant \varepsilon_m < 1$ yields a higher cost per cooperator than c/n_C, whereas $\varepsilon_m > 1$ yields a lower cost. As $\varepsilon_m \to \infty$, the cost per cooperator approaches zero when at least two players cooperate. A lone cooperator always bears the full cost c, since $S(1, \varepsilon_m) = 1$.

To ensure the generality of the model, we apply this general rule by defining distinct synergy factors for interactions on different orders of simplices. Specifically, we introduce a second-order synergy factor, ε_2, for 2-player games on 1-simplices (edges), and a third-order synergy factor, ε_3, for 3-player games on 2-simplices (triangles).

For a 2-player game on an edge (a 1-simplex, group size $G = 2$), the payoffs are determined by the synergy factor ε_2. Let $\Pi^{/}(n_C)$ denote the payoff from such an interaction, $n_C \in \{0, 1, 2\}$. When the synergy factor is ε_2, the corresponding payoffs are

$$\begin{aligned} \Pi_C^{/}(n_C) &= 1 - \frac{r}{S(n_C, \varepsilon_2)}, \quad \text{for } n_C \geqslant 1, \\ \Pi_D^{/}(n_C) &= \begin{cases} 0, & \text{for } n_C = 0, \\ 1, & \text{for } n_C \geqslant 1. \end{cases} \end{aligned} \tag{5}$$

Specifically, the synergy function yields $S(1, \varepsilon_2) = 1$ and $S(2, \varepsilon_2) = 1 + \varepsilon_2$. The defector's payoff remains 1 (if $n_C = 1$) or 0 (if $n_C = 0$).

Similarly, for a 3-player game on a triangle (a 2-simplex, group size $G = 3$), the payoffs, denoted $\Pi^{\Delta}(n_C)$, are governed by the synergy factor ε_3 ($n_C \in \{0, 1, 2, 3\}$):

$$\begin{aligned} \Pi_C^{\Delta}(n_C) &= 1 - \frac{r}{S(n_C, \varepsilon_3)}, \quad \text{for } n_C \geqslant 1, \\ \Pi_D^{\Delta}(n_C) &= \begin{cases} 0, & \text{for } n_C = 0, \\ 1, & \text{for } n_C \geqslant 1. \end{cases} \end{aligned} \tag{6}$$

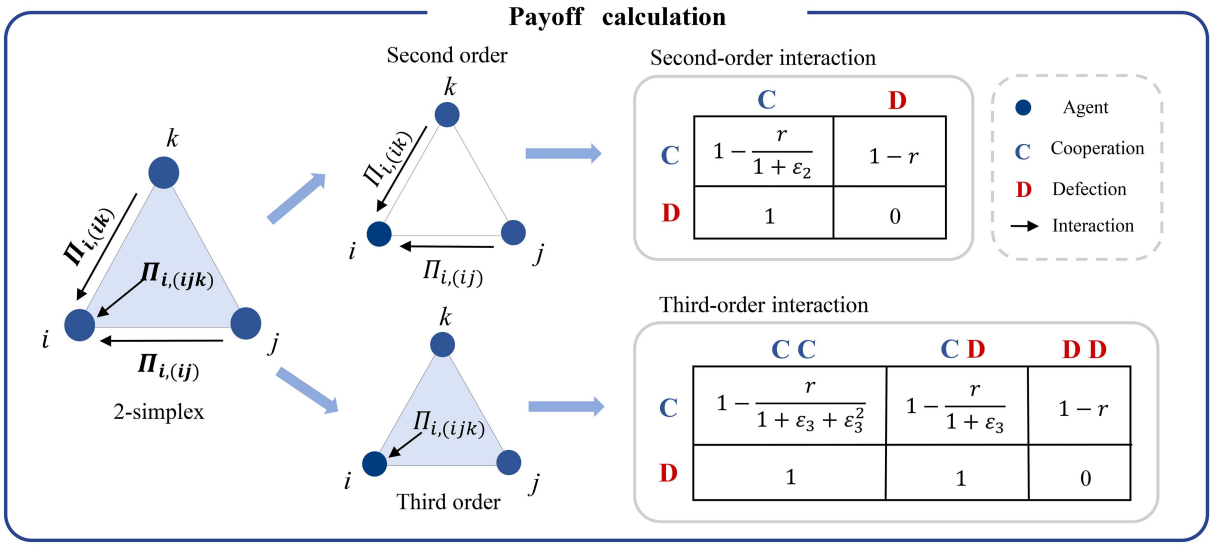

Figure 1 (Color online) Payoff calculation diagram of the nonlinear multiplayer snowdrift game. A 2-simplex contains both second-order and third-order interactions. For the focal agent i, the diagram separates the payoffs from its two incident edges, (i, j) and (i, k), and from the triangle (i, j, k). The corresponding payoff matrices are shown on the right. Rows represent the strategy of i, while columns represent the strategy of the other player or the strategy combinations of the other two players. r denotes the cost-benefit ratio, while ε_2 and ε_3 are nonlinear synergy factors for second-order and third-order interactions, respectively.

Here, $S(1, \varepsilon_3) = 1$, $S(2, \varepsilon_3) = 1 + \varepsilon_3$, and $S(3, \varepsilon_3) = 1 + \varepsilon_3 + \varepsilon_3^2$, corresponding to the scenarios of one cooperator, two cooperators, and three cooperators, respectively.

A single 2-simplex contains both second-order and third-order interactions, and the payoff matrices for these two types of interactions are also intuitively presented in Figure 1. In summary, the total payoff of participant i consists of two parts: second-order interactions and third-order interactions. One part comes from all second-order interactions it participates in, and the other part comes from all third-order interactions it participates in

$$\Pi_i = \sum_{j \in N_i} \Pi^{/}_{i,(ij)} + \sum_{(j,k) \in \triangle_i} \Pi^{\triangle}_{i,(ijk)}. \tag{7}$$

Here, N_i denotes the set of neighbors directly connected to node i via edges, and $\Pi^{/}_{i,(ij)}$ represents the second-order interaction payoff of node i on edge (ij). $\triangle_i$ denotes the set of triangles containing node i, and $\Pi^{\triangle}_{i,(ijk)}$ represents the third-order interaction payoff of node i in the specific triangle (ijk).

2.3 Evolutionary process

We model the evolution of cooperation using a Monte Carlo simulation process. The simulation begins with a population of $N - 1$ defectors and a single cooperator, which is placed at a randomly chosen node. This initial setup allows us to measure the invasion probability of cooperation. Each time step consists of two phases: payoff calculation and strategy update. All individuals first obtain payoffs Π_i by participating in games, and then a random individual i is chosen from the population to update its strategy.

In the strategy update phase, we implement the death-birth (DB) process, where a randomly selected individual i (the "death" event) is replaced by an offspring of one of its neighbors j (the "birth" event), with the selection of j being dependent on its fitness and interaction frequency. The probability that individual i imitates individual j is proportional to the product of j's fitness F_j and the interaction frequency r_{ij}. In this paper, the fitness is mapped from the payoff using the function $F_i = \exp(\theta \Pi_i)$, where θ is the selection intensity. We focus primarily on the weak selection scenario ($0 < \theta \leqslant 1$) [71], where strategic success provides a fitness advantage but does not completely dominate random drift. The strength of the connection between two neighbors i and j is quantified by r_{ij}, which reflects the multiplicity of their interactions. A larger r_{ij} indicates more frequent interactions. On this basis, the probability that individual i chooses to imitate neighbor j is then given by

$$P_{i \leftarrow j} = \frac{F_j r_{ij}}{\sum_{k \in N_i} F_k r_{ik}}, \tag{8}$$

where N_i is the neighbor set of individual i. This imitation probability is thus proportional to both fitness and the strength of their social tie. In the absence of mutations, this evolutionary process is an absorbing Markov chain that will eventually reach one of two absorbing states: all-cooperation (all nodes are cooperators) or all-defection. Our primary metric for the success of cooperation is the fixation probability, denoted ρ_C. This represents the probability that a single cooperator invades an all-defector network system and eventually spreads the cooperation strategy to the entire population. To evaluate the effect of natural selection, we compare ρ_C to the fixation probability under neutral drift, which is simply $1/N$ for a single initial mutant. Selection is said to favor cooperation if $\rho_C > 1/N$. For more intuitive comparisons, we report the normalized fixation probability, $N_{\rho_C} = N \times \rho_C$. Thus, a value of $N_{\rho_C} > 1$ indicates that cooperation is evolutionarily advantageous under the given conditions.

3 Results

In this section, we use Monte Carlo simulations to examine how nonlinear cost sharing affects cooperation fixation. We first analyze the effects of ε_2, ε_3, and network size, and assess sensitivity to selection intensity. We then examine degree heterogeneity, the growth of cooperative clusters, and the effect of the initial cooperator's degree on fixation. Finally, we test whether the main trends persist on simplicial complex networks generated by preferential attachment and on four empirical higher-order networks.

3.1 Impact of synergy factors and network size

To systematically evaluate the impact of nonlinear synergy effects on the evolutionary dynamics of cooperation in higher-order networks, we first examine the dependence of the normalized fixation probability N_{ρ_C} on the dilemma strength r and the nonlinear synergy factors ε_2 and ε_3. Figure 2 illustrates the variation of N_{ρ_C} as a function of r under different parameter combinations. For $(\varepsilon_2, \varepsilon_3) = (1, 1)$, $S(n_C, 1) = n_C$, and the model reduces to the conventional equal cost-sharing multiplayer snowdrift game. Relative to this baseline, raising ε_2 in Figure 2(a) or ε_3 in Figure 2(c) shifts N_{ρ_C} upward and moves the intersection with the neutral-drift line to a higher r, thereby increasing r^*. Notably, when both second-order and third-order synergy factors are enhanced simultaneously ($\varepsilon_2 > 1, \varepsilon_3 > 1$), N_{ρ_C} is further elevated, demonstrating a synergistic promotion effect. The reason for this promotion lies in the fact that the nonlinear synergy mechanism alters the way cooperative costs are shared: when multiple cooperators exist in a group, as ε_2 and ε_3 increase, the effective cost actually borne by each cooperator decreases, thereby making it easier for cooperation to gain a payoff advantage.

Figure 2 demonstrates the enhancing effect of nonlinear synergy factors on the level of cooperation. To quantitatively characterize this promotion effect, Figure 3 illustrates the variation of the critical cost-benefit ratio r^* for cooperation evolution with the nonlinear synergy factors ε_2 and ε_3. Specifically, Figures 3(a) and (b) show the increasing trend of r^* with respect to ε_2 for fixed ε_3 values of 1 and 2, respectively. Similarly, Figures 3(c) and (d) fix ε_2 to 1 and 2, respectively, displaying the variation of r^* with ε_3. The results indicate that under all parameter settings, r^* increases with the growth of nonlinear synergy factors, meaning the range of cost-benefit ratios where cooperative strategies dominate is expanded. This trend holds for both second-order and third-order synergy factors, demonstrating that enhancing the nonlinear synergy effect at any level can effectively promote the evolution of cooperation. To determine whether this trend persists beyond the range shown in the main panels, the insets plot r^* at $\varepsilon_m = 0.1, 1, 10$, and 100 on a logarithmic horizontal axis. For both network sizes and all four fixed-factor settings, r^* continues to increase with the varied synergy factor. The increase from 10 to 100, however, is smaller than that from 1 to 10. This reduced sensitivity is consistent with the cost-sharing rule: when several players cooperate, their individual costs are already small at high synergy, so further increases in ε_m have a weaker effect on r^*. A second key observation from Figure 3 is the consistent impact of network size. The influence of network size on the critical cost-benefit ratio is further observed in Figure 3: under identical synergy factors, the r^* value for the larger network ($N = 100$) is consistently higher than that for the smaller network ($N = 80$), indicating that cooperation is more readily established in larger populations under our model's conditions.

To further investigate the impact of network size on cooperation evolution, we explore this relationship more directly in Figure 4, which plots the full cooperation evolution curves (N_{ρ_C} vs. r) for five different network sizes. The results confirm the trend observed in Figure 3 in greater detail that both the overall normalized fixation probability (N_{ρ_C}) and the critical threshold (r^*) increase monotonically with network size. The underlying mechanism for this size effect is rooted in our network generation model. Under the triangle-growth rule, larger networks contain a greater number of 2-simplices. This structural richness provides more opportunities for individuals, especially high-degree nodes, to engage in multiplayer games where strong nonlinear synergies can be realized. Consequently,

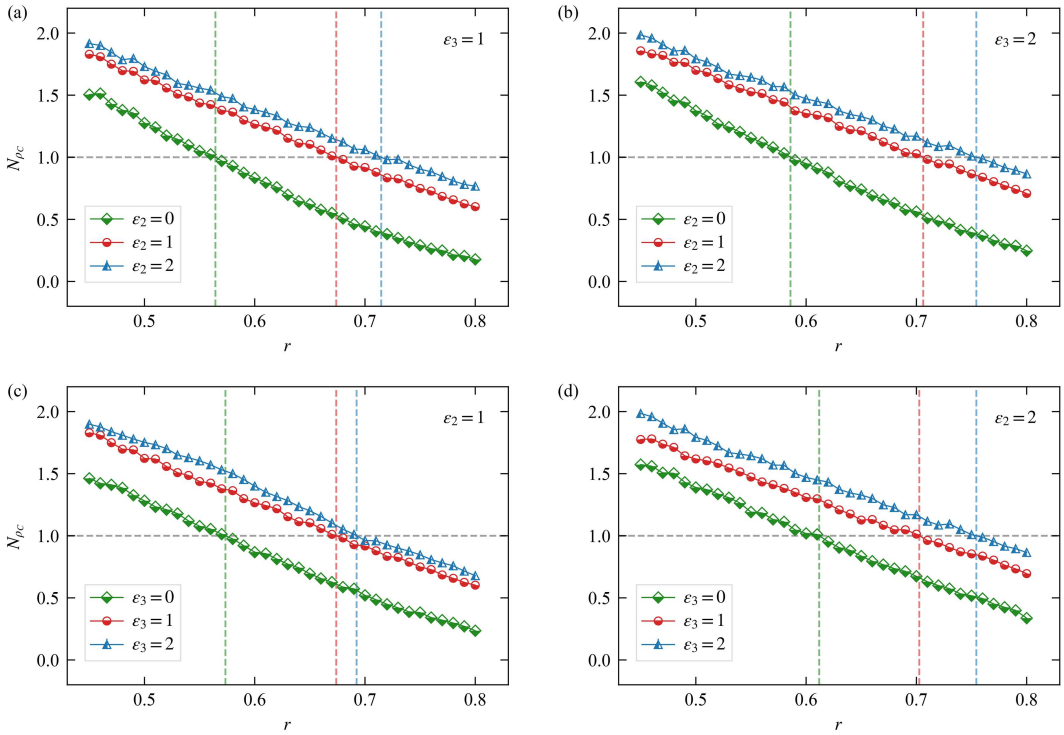

Figure 2 (Color online) Variation of the normalized fixation probability N_{ρ_C} with dilemma strength r and nonlinear synergy factors ε_2 and ε_3. (a) and (b) compare different ε_2 at fixed $\varepsilon_3 = 1$ and 2, respectively, whereas (c) and (d) compare different ε_3 at fixed $\varepsilon_2 = 1$ and 2. The $\varepsilon_2 = 1$ curve in (a) and the $\varepsilon_3 = 1$ curve in (c) both represent $(\varepsilon_2, \varepsilon_3) = (1, 1)$, the conventional equal cost-sharing case. The horizontal dashed line $N_{\rho_C} = 1$ represents the neutral drift baseline, and the colored vertical dashed lines mark the intersection points of the curves with this baseline. The r value corresponding to each intersection is defined as the critical cost-benefit ratio r^* for the evolution of cooperation. As either synergy factor increases, the curves shift upward and r^* moves to larger values, indicating that cooperation is favored over a wider range of cost-benefit ratios. The cooperation fixation probability is determined by the proportion of times that cooperators reach an absorbing state in 10^6 simulations. Parameter settings: $N = 100$, $\theta = 0.05$.

larger networks create a more fertile ground for the evolution of cooperation, amplifying the benefits of the nonlinear payoff structure.

Based on the aforementioned findings, Figure 5 presents a three-dimensional phase diagram to comprehensively illustrate the combined effects of network size N and nonlinear synergy factors (ε_2 and ε_3) on the critical cost-benefit ratio r^*. The figure visually confirms our primary conclusion. It can be seen that r^* increases monotonically with all three parameters. This is evident as the surfaces consistently rise along the axes for N, ε_2, and ε_3, which indicates that both the expansion of the network scale and the enhancement of nonlinear synergy effects significantly broaden the parameter space conducive to the evolution of cooperation. Furthermore, in both panels, the red surface (representing a higher baseline synergy) is consistently elevated above the gray surface. This visualization provides a powerful map of the conditions that favor cooperation. The highest values of r^*, representing the most robust cooperative regime, are found in the region where network size, second-order synergy, and third-order synergy are all maximized (the top-right-front corner of the red surfaces). The phase diagram demonstrates that these factors do not merely have additive effects, but reinforce one another, creating a landscape where large networks with strong nonlinear synergies become exceptionally fertile ground for the evolution of cooperation.

Following the weak-selection perspective adopted in this study [71], we examine the effect of selection intensity on cooperation for $0 < \theta \leqslant 1$. Figure 6 shows the variation of the normalized fixation probability N_{ρ_C} with θ under different combinations of ε_2 and ε_3. In Figures 6(a) and (b), ε_2 varies at fixed $\varepsilon_3 = 1$ and 2, respectively; in Figures 6(c) and (d), ε_3 varies at fixed $\varepsilon_2 = 1$ and 2. Within the examined range, N_{ρ_C} generally increases with θ, although the increase becomes less pronounced toward the upper end of the range. At a given θ, larger ε_2 or ε_3 generally corresponds to a higher fixation probability. These results show that the cooperation-promoting effect of increasing either synergy factor is also observed near the weak-selection reference setting $\theta = 0.05$, motivating a closer examination of how degree heterogeneity contributes to this effect.

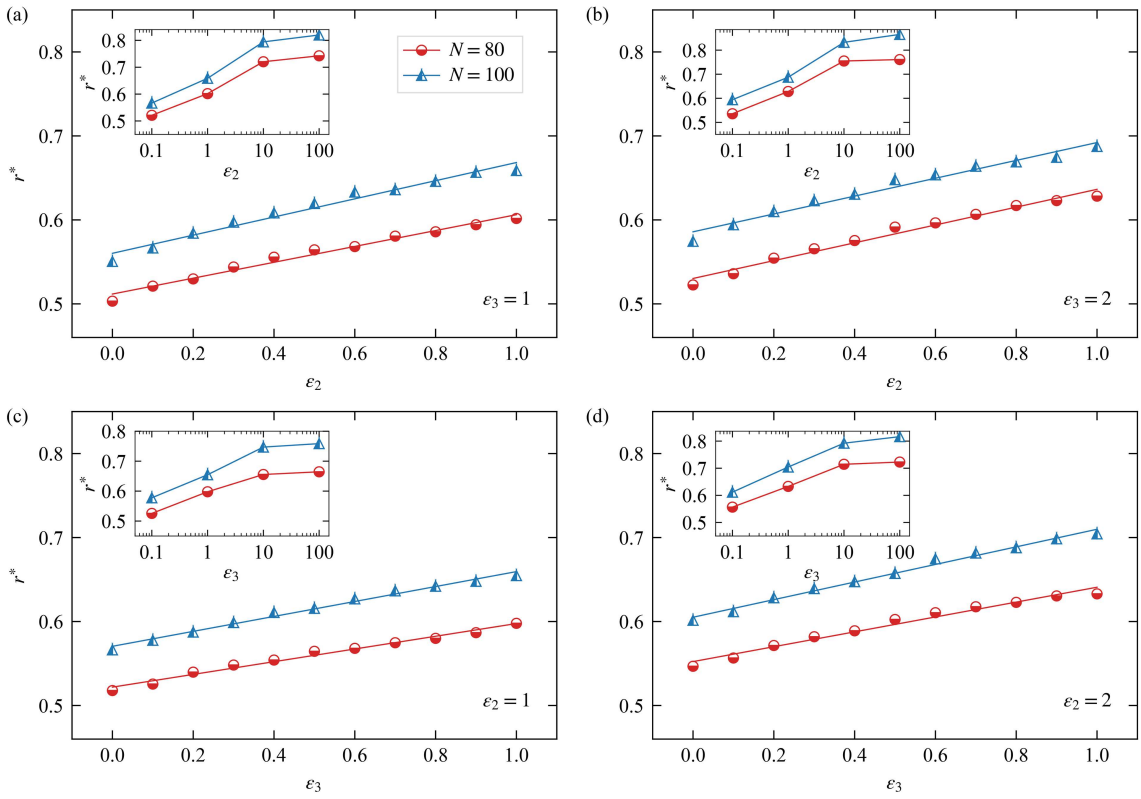

Figure 3 (Color online) Variation of the critical cost-benefit ratio r^* for cooperation evolution with nonlinear synergy factors ε_2 and ε_3. (a) and (b) fix $\varepsilon_3 = 1$ and $\varepsilon_3 = 2$, respectively, showing the change in r^* with ε_2. (c) and (d) fix $\varepsilon_2 = 1$ and $\varepsilon_2 = 2$, respectively, displaying the change in r^* with ε_3. The inset in each panel shows r^* at $\varepsilon_m = 0.1, 1, 10$, and 100 for the varied factor on a logarithmic horizontal axis. Different colors and markers correspond to different network sizes $N \in \{80, 100\}$. In each panel, r^* rises with the varied synergy factor and is higher for $N = 100$ than for $N = 80$, showing that stronger synergy and larger network size both extend the parameter range favoring cooperation. All other model settings and parameter values are consistent with those in Figure 2.

3.2 Degree heterogeneity and the formation mechanism of local cooperative clusters

Previous findings have confirmed that increasing the synergy factors promotes cooperation, but the underlying mechanism requires further investigation. We approach this from the perspective of node degree heterogeneity, examining the strategy selection preferences of nodes with different degrees during the evolutionary process.

Figure 7(a) illustrates the relationship between node degree and its cooperation time proportion, defined as the fraction of total evolutionary steps a node spends in the cooperative state. Specifically, we counted the number of time steps during which each individual node adopted the cooperative strategy (C) and its total evolutionary time steps, and calculated the time proportion of cooperation for each node (i.e., the ratio of the steps in which the node chose C to the total evolutionary steps). All nodes were then grouped by their degree, and the average time proportion of cooperation among nodes with the same degree was taken as the value for that degree. The results show that the time proportion of cooperation generally increases with node degree, indicating that high-degree nodes exhibit a significantly higher proportion of cooperation than low-degree nodes. Notably, when the nonlinear synergy effect is strengthened (from $(\varepsilon_2, \varepsilon_3) = (1, 1)$ to $(2, 2)$), the difference in the cooperation time proportion between nodes of different degrees is markedly amplified, and the advantage of high-degree nodes in maintaining cooperation becomes more pronounced. High-degree nodes (i.e., the top 25% of nodes by ordinary degree) transition from being occasional cooperators to robust anchors of cooperation. This occurs because high-degree nodes participate in a larger number of group interactions; under the nonlinear cost-sharing mechanism, reduced costs in interactions involving multiple cooperators can enhance their cumulative payoff advantage, helping them maintain cooperation.

To understand how these high-degree cooperators influence the rest of the population, we explore the local environment surrounding them. Figure 7(b) shows the temporal evolution of the proportion of cooperative neighbors around high-degree nodes (i.e., the top 25% of nodes by ordinary degree) when these high-degree nodes adopt different strategies. A stark contrast emerges based on the high-degree node's own strategy: when a high-degree node adopts cooperation, the proportion of cooperative neighbors around it increases rapidly and eventually reaches a high steady-state level. In contrast, when a high-degree node adopts the defection strategy, the proportion

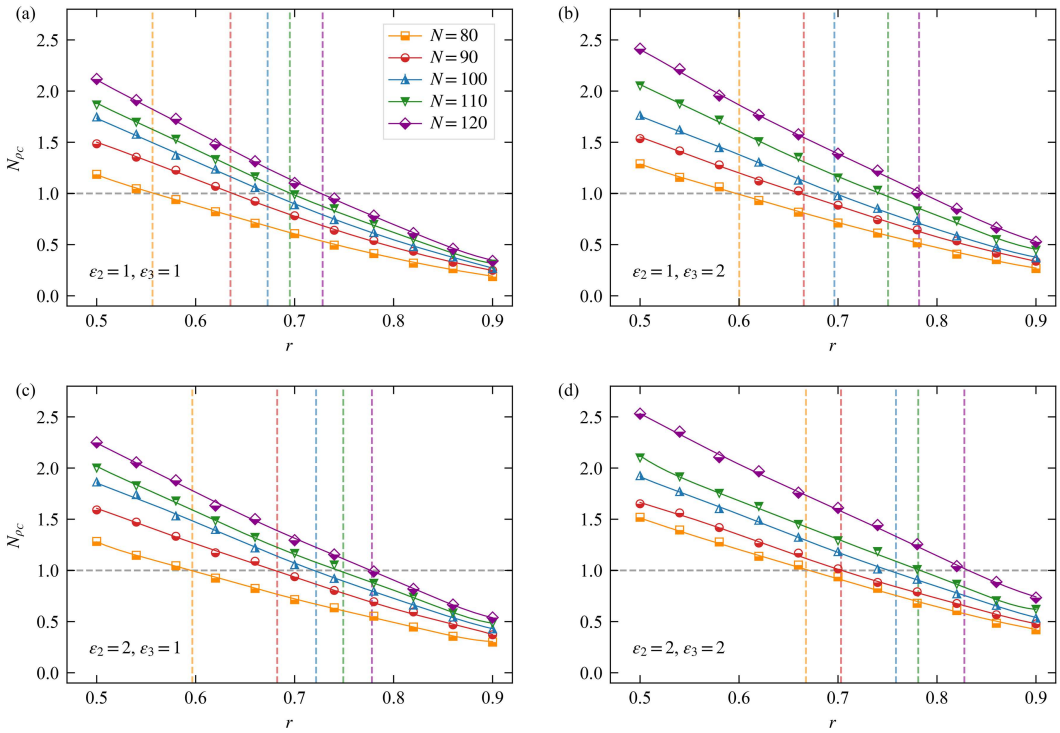

Figure 4 (Color online) Variation of the normalized fixation probability $N_{\rho C}$ with dilemma strength r under different network sizes. The four subplots correspond to different parameter combinations: $(\varepsilon_2, \varepsilon_3) \in \{(1,1),(1,2),(2,1),(2,2)\}$, and different colors and markers represent different network sizes $N \in \{80, 90, 100, 110, 120\}$. The horizontal dashed line denotes neutral drift ($N_{\rho C} = 1$), while the colored vertical dashed lines indicate the corresponding critical values r^*. Across all four parameter combinations, increasing N raises $N_{\rho C}$ and shifts r^* to larger values, further supporting the network-size effect observed in Figure 3. All other model settings and parameter values are consistent with those in Figure 2.

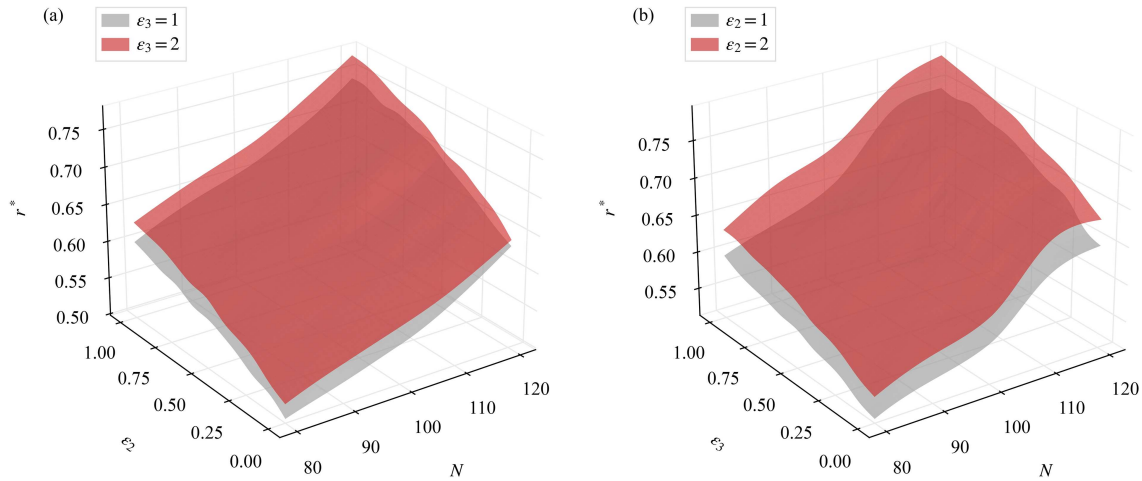

Figure 5 (Color online) Three-dimensional phase diagram of the critical cost-benefit ratio r^* with respect to network size N and synergy factors ε_2 and ε_3. (a) fixes ε_3, showing the variation of r^* with N and ε_2, where the two surfaces correspond to $\varepsilon_3 = 1$ (gray) and $\varepsilon_3 = 2$ (red), respectively. (b) fixes ε_2, displaying the variation of r^* with N and ε_3, where the two surfaces correspond to $\varepsilon_2 = 1$ (gray) and $\varepsilon_2 = 2$ (red), respectively. The network size ranges over $N \in \{80, 90, 100, 110, 120\}$. All other model settings and parameter values are consistent with those in Figure 2.

of cooperative neighbors around it remains consistently low. This demonstrates that the cooperative strategy can induce the formation of local cooperative clusters around high-degree nodes, whereas the defection strategy cannot achieve such a local aggregation effect. More importantly, when the nonlinear synergy effect is enhanced, the proportion of cooperative neighbors around high-degree nodes adopting the cooperative strategy increases significantly.

In summary, the results in Figure 7 reveal the key mechanism of high-degree nodes in cooperation evolution.

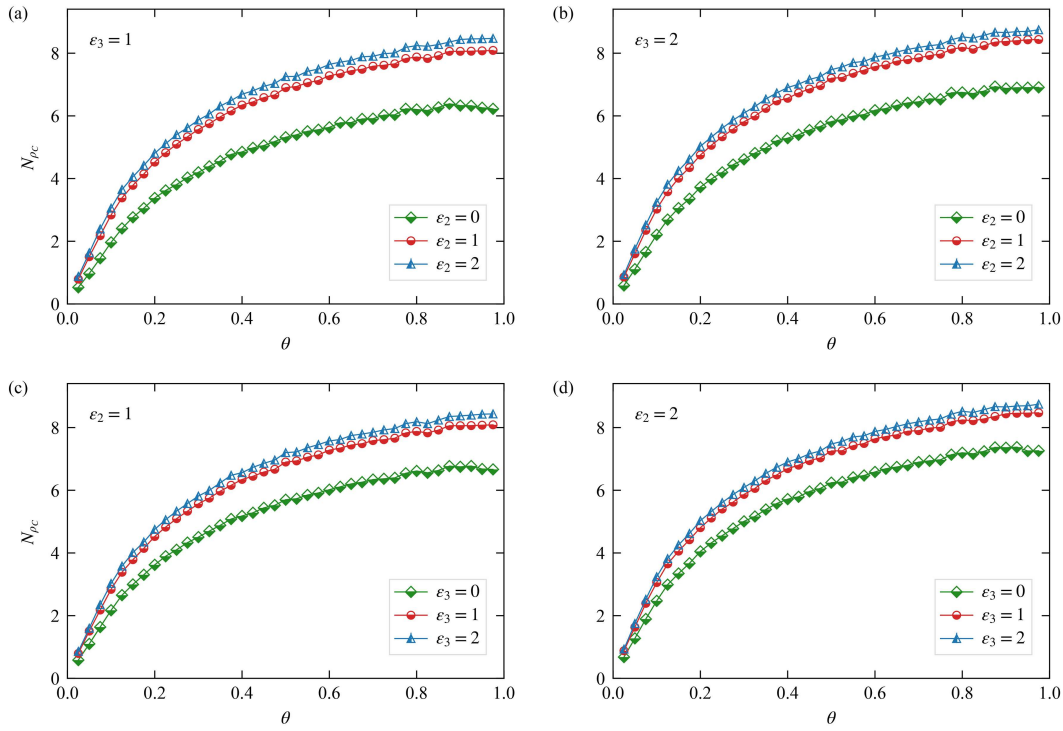

Figure 6 (Color online) Variation of the normalized fixation probability $N_{\rho C}$ with selection intensity θ under different nonlinear synergy factors. (a) and (b) compare $\varepsilon_2 \in \{0, 1, 2\}$ at fixed $\varepsilon_3 = 1$ and 2, respectively, whereas (c) and (d) compare $\varepsilon_3 \in \{0, 1, 2\}$ at fixed $\varepsilon_2 = 1$ and 2, respectively. Each data point is based on 10^6 independent runs. Parameter settings: $N = 100$, $r = 0.6$.

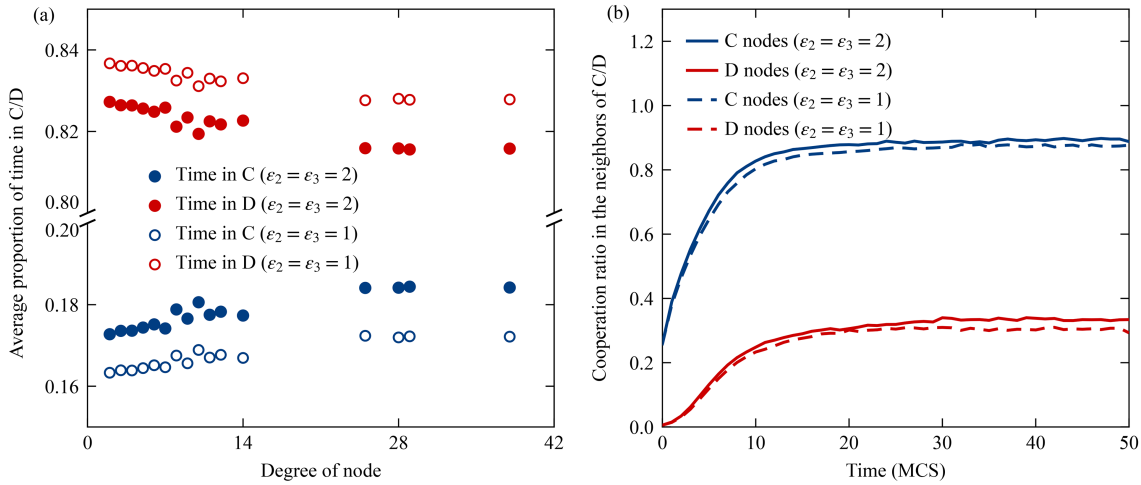

Figure 7 (Color online) The influence of degree heterogeneity on the evolution of cooperation. (a) shows the relationship between node degree and the average proportion of time spent in cooperation or defection, where hollow circles represent $(\varepsilon_2, \varepsilon_3) = (1, 1)$ and solid circles represent $(\varepsilon_2, \varepsilon_3) = (2, 2)$; blue indicates the cooperation strategy, and red indicates the defection strategy. (b) shows the temporal evolution of the proportion of cooperative neighbors around high-degree nodes (i.e., the top 25% of nodes by ordinary degree) when they adopt different strategies: dashed lines correspond to $(\varepsilon_2, \varepsilon_3) = (1, 1)$ and solid lines correspond to $(\varepsilon_2, \varepsilon_3) = (2, 2)$; blue denotes high-degree cooperators (C) and red denotes high-degree defectors (D). Parameter settings: $N = 100$, $r = 0.5$, $\theta = 0.05$.

When a high-degree node adopts the cooperative strategy, its participation in multiple game interactions allows it to accumulate a significant payoff advantage through the nonlinear cost-sharing mechanism. This payoff advantage, via the fitness-based strategy update mechanism, makes it easier to attract neighboring nodes to switch to cooperation, forming local cooperative clusters centered on high-degree cooperative nodes. The formation of local cooperative clusters, in turn, provides a sustained high-payoff environment for high-degree cooperators, creating a positive feedback loop that enhances the relative stability of the cooperative strategy in high-degree nodes.

To intuitively demonstrate the driving role of high-degree nodes in cooperation evolution, Figure 8 presents two sequences of snapshots depicting the cooperation evolution process. In the early stage of evolution, a single

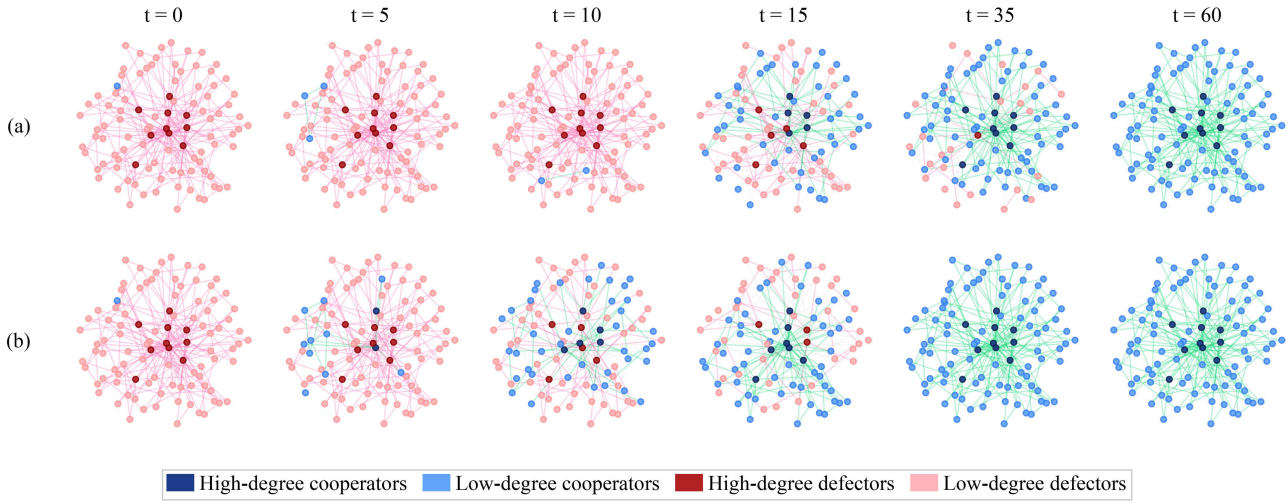

Figure 8 (Color online) Snapshots of cooperation evolution. (a) corresponds to $(\varepsilon_2, \varepsilon_3) = (1, 1)$; (b) corresponds to $(\varepsilon_2, \varepsilon_3) = (2, 2)$. Columns from left to right represent time steps $t = 0, 5, 10, 15, 35, 60$. Node colors indicate the combination of strategy and degree: dark blue represents high-degree cooperators, light blue represents low-degree cooperators, dark red represents high-degree defectors, and light red represents low-degree defectors. Both experiments use the same network structure and initial state (a single cooperator is randomly placed in an all-defector population). Parameter settings: $N = 100$, $r = 0.5$, $\theta = 0.05$.

cooperator enters an all-defector population. When high-degree nodes switch to cooperation, these high-degree cooperators, leveraging their abundant connections, propagate the cooperative strategy to their neighboring nodes, gradually forming cooperative clusters centered on high-degree nodes. Eventually, the cooperative strategy becomes dominant in the network. In this process, high-degree cooperators act as centers of cooperative spread, effectively driving the improvement of cooperation levels in local regions and even the entire network. A comparison between Figure 8(a) with $(\varepsilon_2, \varepsilon_3) = (1, 1)$ and Figure 8(b) with $(\varepsilon_2, \varepsilon_3) = (2, 2)$ reveals that when the synergy factors are increased, cooperation spreads faster, and cooperative clusters form earlier and remain more stable.

To quantify the formation and expansion of the cooperative clusters illustrated in Figure 8, Figure 9 tracks the largest connected cooperative cluster as a fraction of network size during the evolutionary process. The curves are averaged over trajectories that eventually reach full cooperation, allowing us to compare how rapidly successful cooperative invasions spread through the network. In Figure 9(a), with $(\varepsilon_2, \varepsilon_3) = (2, 2)$, the curve for $r = 0.5$ rises fastest, followed by those for $r = 0.6$ and $r = 0.7$. Thus, at a given stage of the invasion, a lower cost-benefit ratio is associated with a larger cooperative cluster. In Figure 9(b), at $r = 0.6$, the cluster grows faster under $(\varepsilon_2, \varepsilon_3) = (2, 2)$ than under the conventional equal cost-sharing case $(1, 1)$. Although the curves ultimately converge as cooperation fixes, their different growth rates show that nonlinear cost sharing affects not only the fixation outcome examined above but also the expansion of cooperative clusters leading to that outcome. These results provide a quantitative counterpart to the evolutionary snapshots in Figure 8.

To further examine whether the initial cooperator's location affects cooperation fixation, Figure 10 compares the conditional normalized fixation probability according to the initial node's ordinary-degree rank. Each simulation starts from an all-defector network and introduces a single cooperator at a randomly selected node. After ranking all nodes by ordinary degree from highest to lowest, we divide them into three groups: the lowest-degree 25%, the middle-degree 50%, and the highest-degree 25%. Figures 10(a) and (b) show the results for $(\varepsilon_2, \varepsilon_3) = (1, 1)$ and $(2, 2)$, respectively. Under both parameter settings, N_{ρ_C} is substantially higher when cooperation starts from a node in the highest-degree 25% than when it starts from a node in the middle-degree 50% or lowest-degree 25%, indicating a clear association between the initial node's degree and the eventual fixation of cooperation. In addition, compared with the $(1, 1)$ case, the curves for $(2, 2)$ are generally higher within each group, suggesting that stronger cost-sharing synergy also favors cooperation fixation across different initial-degree groups. This finding complements the preceding analysis of how high-degree nodes facilitate the spread of cooperation and the formation of local cooperative clusters.

3.3 Robustness across alternative network topologies and empirical networks

The results presented above were obtained on triangle-growth networks with uniform edge selection. To test whether they depend on this selection rule, we also generated simplicial complexes within the same triangle-growth framework using preferential attachment, whereby an existing edge is selected with probability proportional to the

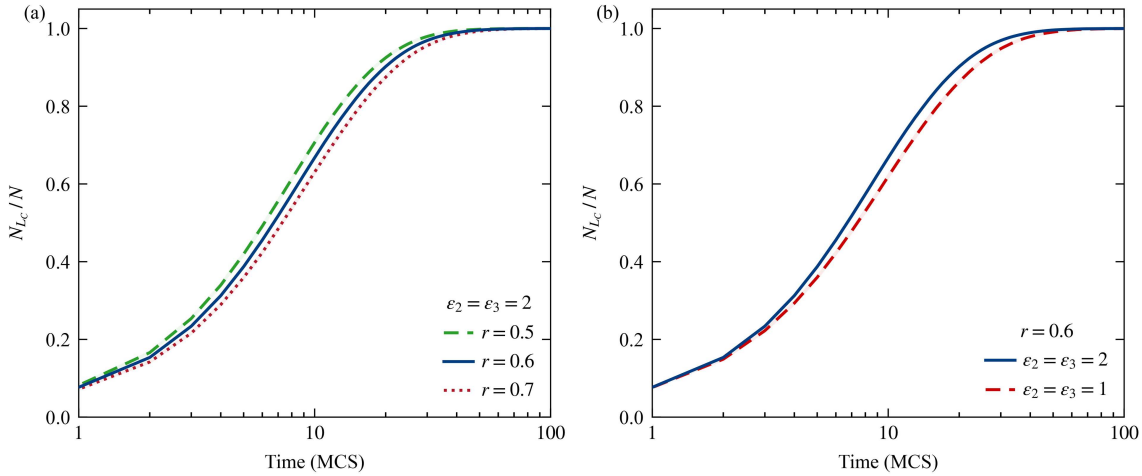

Figure 9 (Color online) Time evolution of the relative size of the largest cooperative cluster N_{L_C}/N. Here, N_{L_C} is the number of nodes in the largest cluster of cooperators connected by edges of the simplicial complex. The curves are averaged over runs that reach full cooperation. (a) compares $r = 0.5$, 0.6 and 0.7 at $(\varepsilon_2, \varepsilon_3) = (2, 2)$; (b) compares $(\varepsilon_2, \varepsilon_3) = (1, 1)$ and $(2, 2)$ at $r = 0.6$. Time is measured in Monte Carlo steps (MCS), with one MCS consisting of N update attempts, and is shown on a logarithmic scale. Parameter settings: $N = 100$, $\theta = 0.05$.

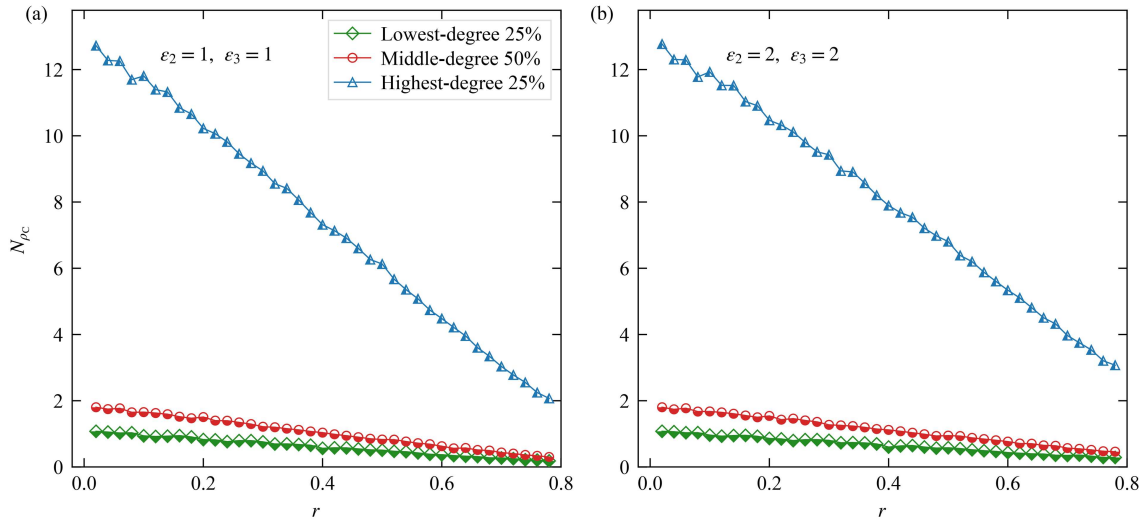

Figure 10 (Color online) Normalized fixation probability N_{ρ_C} as a function of the cost-benefit ratio r for different degrees of the initial cooperator. (a) and (b) correspond to $(\varepsilon_2, \varepsilon_3) = (1, 1)$ and $(2, 2)$, respectively. Green diamonds, red circles, and blue triangles denote initial nodes in the lowest-degree 25%, middle-degree 50%, and highest-degree 25% of the ordinary-degree ranking, respectively. Each curve shows N_{ρ_C} conditional on the initial node's degree group. For each parameter setting and r, 10^6 simulations are classified by initial-degree group. Parameter settings: $N = 100$, $\theta = 0.05$.

sum of the degrees of its two endpoints. The two constructions differ only in edge selection and, at a given network size, retain the same numbers of nodes, edges, and triangles. As shown in Figure 11, increasing either ε_2 or ε_3 raises N_{ρ_C} and shifts the critical cost-benefit ratio r^* to higher values. This trend is consistent with that observed under uniform edge selection, indicating that the cooperation-promoting effect of nonlinear cost sharing is not confined to the original attachment rule.

We further examine the findings on empirical higher-order networks. We conducted experiments on four real datasets: (a) the Email-Enron network with $N = 91$ and $\langle k \rangle = 4.9$ [72], (b) a Coauth-DBLP subset with $N = 100$ and $\langle k \rangle = 3.1$ [72], (c) the Hospital-Lyon contact network with $N = 46$ and $\langle k \rangle = 7$ [73], and (d) the Primary School contact network with $N = 223$ and $\langle k \rangle = 7$ [74, 75]. These datasets cover diverse interaction scenarios, including social communication, academic collaboration, and face-to-face contact, and exhibit different network sizes and topological characteristics. Each dataset was processed into a subnetwork containing only interaction records with exactly three participants; groups larger than three were not included, so that every retained record defines one 2-simplex and the three pairwise links among its participants.

Figure 12 illustrates the variation of the normalized fixation probability N_{ρ_C} with dilemma strength r across the

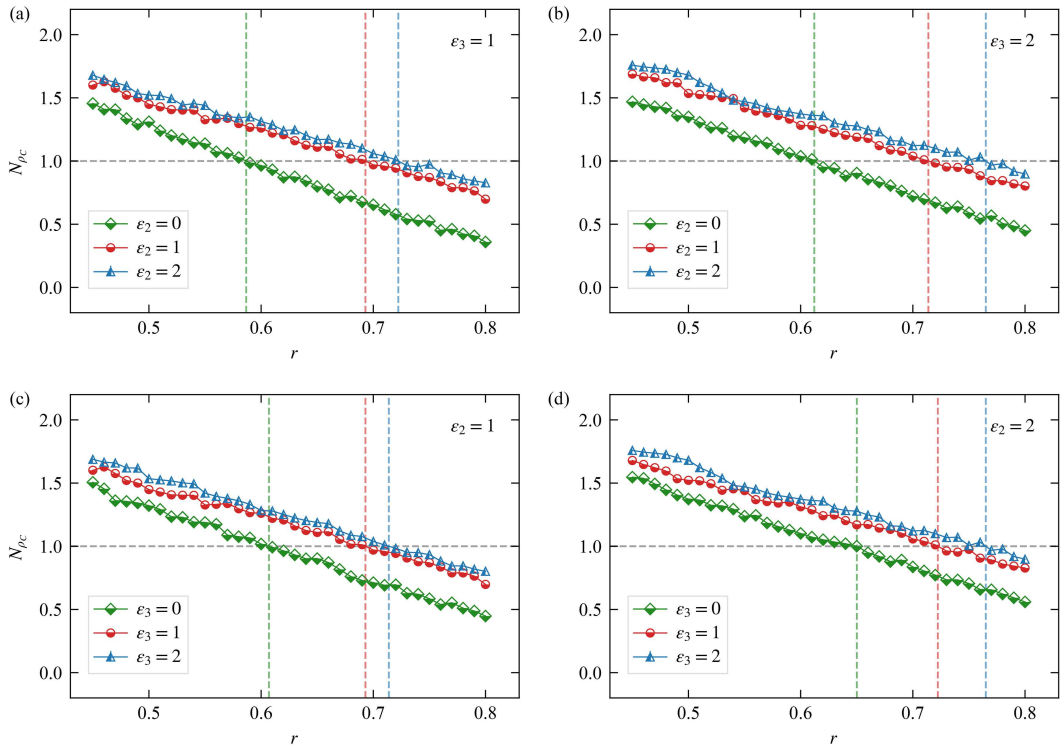

Figure 11 (Color online) Variation of the normalized fixation probability N_{ρ_C} with dilemma strength r on preferential-attachment simplicial complex networks. (a) and (b) compare different ε_2 at fixed $\varepsilon_3 = 1$ and 2, respectively, while (c) and (d) compare different ε_3 at fixed $\varepsilon_2 = 1$ and 2. The horizontal dashed line denotes the neutral drift baseline $N_{\rho_C} = 1$, and the colored vertical dashed lines mark the critical cost-benefit ratios r^*. Each data point is based on 10^6 independent runs. Parameter settings: $N = 100$, $\theta = 0.05$.

four real-world networks. It can be observed that in all datasets, increasing either the second-order or third-order synergy factor shifts the $N_{\rho C}$ curve upward and moves the critical cost-benefit ratio r^* for cooperation evolution to the right; when both the second-order and third-order synergy factors are enhanced simultaneously ($\varepsilon_2 = 2, \varepsilon_3 = 2$), the cooperation promotion effect is most significant. Despite the differences in the origin, size, and topology of the four networks, the promoting effect of nonlinear synergy on cooperation evolution is validated across all networks, showing a consistent pattern. These results indicate that the nonlinear synergy mechanism's promoting effect on cooperation evolution has broad applicability, independent of specific network structure.

4 Conclusion

This study develops a nonlinear cost-sharing rule for multiplayer snowdrift games on simplicial complex networks. The order-specific synergy factors ε_2 and ε_3 determine how each cooperator's cost varies with the number of cooperators in second- and third-order interactions, respectively. Using death-birth updating, we examine cooperation fixation across different synergy factors, network sizes, selection intensities, and initial cooperator degree groups. We also test the main trends on simplicial complex networks generated by preferential attachment and on four empirical higher-order networks.

Increasing either synergy factor raises the normalized fixation probability and shifts the critical cost-benefit ratio r^* to higher values, expanding the range favorable to cooperation. This trend persists across the selection intensities and network structures examined. The degree-based analyses associate high-degree nodes with greater local cooperation and higher conditional fixation probability when selected as the initial cooperator. Among trajectories that reach full cooperation, stronger synergy also accelerates the growth of the largest cooperative cluster. Together, these results show how nonlinear cost sharing affects both the fixation and spatial spread of cooperation in the networks studied.

Future research can be extended in several promising directions: first, by generalizing the model to a broader range of higher-order structures, such as hypergraphs and simplicial complexes with diverse generative mechanisms, to further validate the robustness of nonlinear synergy effects across varied topologies; second, by incorporating alternative strategy update rules, such as self-interactive learning and reinforcement learning, to investigate how

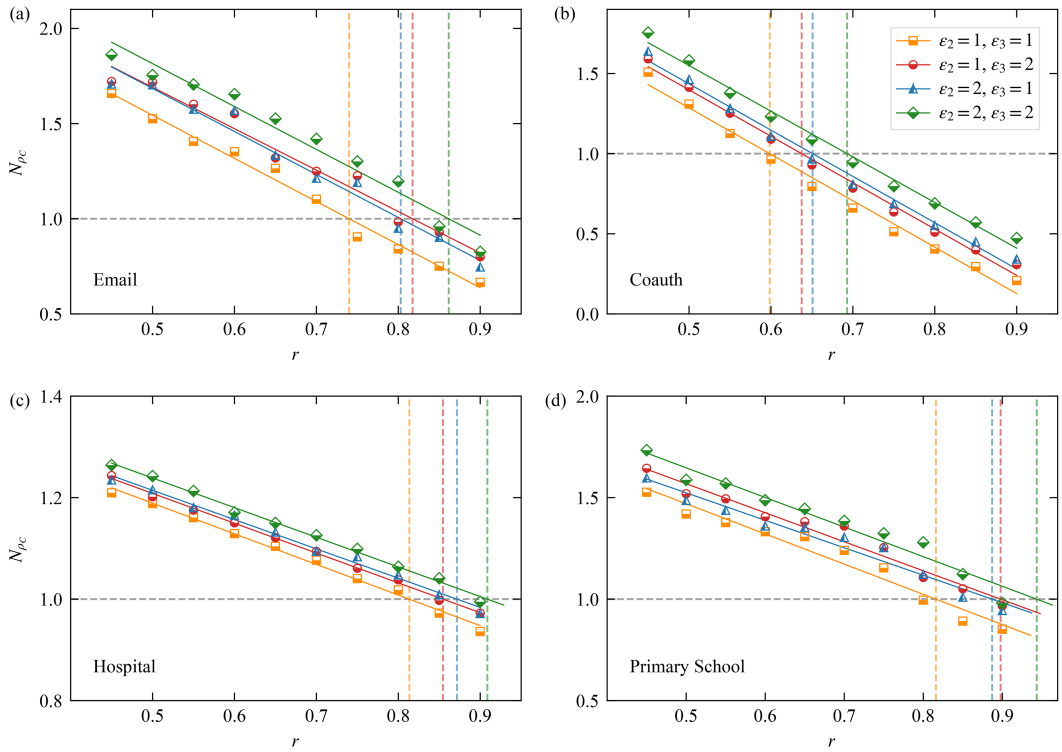

Figure 12 (Color online) Variation of the normalized fixation probability N_{ρ_C} with dilemma strength r across four real-world higher-order network datasets. The four subplots correspond to (a) email-Enron ($N = 91$), (b) coauth-DBLP ($N = 100$), (c) hospital-lyon ($N = 46$), and (d) primary school ($N = 223$). Different colors and markers represent different parameter combinations: $(\varepsilon_2, \varepsilon_3) \in \{(1,1),(1,2),(2,1),(2,2)\}$. The horizontal dashed line denotes the neutral drift baseline $N_{\rho_C} = 1$, and the colored vertical dashed lines mark the critical cost-benefit ratio r^* for each parameter combination. Each data point shows the normalized fixation probability $N_{\rho_C} = N\rho_C$, where ρ_C is estimated as the fraction of 10^6 independent runs that reach the all-cooperator absorbing state.

different evolutionary dynamics influence the emergence and maintenance of cooperation; and finally, by exploring the co-evolutionary dynamics between network topology and game strategies, specifically examining the mechanisms through which individuals adaptively adjust their social connections based on game outcomes.

Acknowledgements This work was supported by National Natural Science Foundation of China (Grant Nos. 12565005, 72501127), Guangxi Science and Technology Base and Talent Special Project (Grant No. AD25069071), and Open Project of Key Laboratory of Mathematics and Information Networks (Beijing University of Posts and Telecommunications), Ministry of Education, China (Grant No. KF202402). Tina P. BENKO and Matjaž PERC were supported by the Slovenian Research and Innovation Agency (Grant Nos. P5-0024, P1-0403).

References

1 Fehr E, Gächter S. Altruistic punishment in humans. Nature, 2002, 415: 137–140
2 Nowak M A. Five rules for the evolution of cooperation. Science, 2006, 314: 1560–1563
3 Fehr E, Fischbacher U. Social norms and human cooperation. Trends Cogn Sci, 2004, 8: 185–190
4 Axelrod R, Hamilton W D. The evolution of cooperation. Science, 1981, 211: 1390–1396
5 Perc M, Jordan J J, Rand D G, et al. Statistical physics of human cooperation. Phys Rep, 2017, 687: 1–51
6 Van Lange P A M, Joireman J, Parks C D, et al. The psychology of social dilemmas: a review. Organ Behav Hum Dec, 2013, 120: 125–141
7 Zeng Z, Feng M, Szolnoki A. Evolutionary dynamics with self-interaction learning in networked systems. IEEE Trans Netw Sci Eng, 2026, 13: 296–313
8 Wang S, Liu J. A multi-objective evolutionary algorithm for promoting the emergence of cooperation and controllable robustness on directed networks. IEEE Trans Netw Sci Eng, 2018, 5: 92–100
9 Allen B, Lippner G, Chen Y T, et al. Evolutionary dynamics on any population structure. Nature, 2017, 544: 227–230
10 Wang S, Yao W, Cao M, et al. Evolutionary dynamics under periodic switching of update rules on regular networks. IEEE Trans Netw Sci Eng, 2024, 11: 1337–1346
11 Sun Z, Chen X, Szolnoki A. State-dependent optimal incentive allocation protocols for cooperation in public goods games on regular networks. IEEE Trans Netw Sci Eng, 2023, 10: 3975–3988
12 Zhang Y, Wang J, Wen G, et al. Limitation of time promotes cooperation in structured collaboration systems. IEEE Trans Netw Sci Eng, 2025, 12: 4–12

13 Musciotto F, Battiston F, Mantegna R N. Detecting informative higher-order interactions in statistically validated hypergraphs. Commun Phys, 2021, 4: 218

14 Majhi S, Perc M, Ghosh D. Dynamics on higher-order networks: a review. J R Soc Interface, 2022, 19: 20220043

15 Perc M, Gómez-Gardeñes J, Szolnoki A, et al. Evolutionary dynamics of group interactions on structured populations: a review. J R Soc Interface, 2013, 10: 20120997

16 Battiston F, Cencetti G, Iacopini I, et al. Networks beyond pairwise interactions: structure and dynamics. Phys Rep, 2020, 874: 1–92

17 Iacopini I, Petri G, Barrat A, et al. Simplicial models of social contagion. Nat Commun, 2019, 10: 2485

18 Battiston F, Amico E, Barrat A, et al. The physics of higher-order interactions in complex systems. Nat Phys, 2021, 17: 1093–1098

19 Boccaletti S, De Lellis P, del Genio C I, et al. The structure and dynamics of networks with higher order interactions. Phys Rep, 2023, 1018: 1–64

20 Broom M, Rychtář J. A general framework for analysing multiplayer games in networks using territorial interactions as a case study. J Theor Biol, 2012, 302: 70–80

21 Li A, Broom M, Du J, et al. Evolutionary dynamics of general group interactions in structured populations. Phys Rev E, 2016, 93: 022407

22 Su Q, Zhou L, Wang L. Evolutionary multiplayer games on graphs with edge diversity. PLoS Comput Biol, 2019, 15: e1006947

23 Gokhale C S, Traulsen A. Evolutionary multiplayer games. Dyn Games Appl, 2014, 4: 468–488

24 Peña J, Nöldeke G. Group size effects in social evolution. J Theor Biol, 2018, 457: 211–220

25 Peña J. Group-size diversity in public goods games. Evolution, 2012, 66: 623–636

26 Wei M, Wang X, Liu L, et al. Indirect reciprocity in the public goods game with collective reputations. J R Soc Interface, 2025, 22: 20240827

27 Peña J, Wu B, Arranz J, et al. Evolutionary games of multiplayer cooperation on graphs. PLoS Comput Biol, 2016, 12: e1005059

28 Wang D, Yi P, Yan G, et al. Evolutionary dynamics of pairwise and group cooperation in heterogeneous social networks. IEEE Trans Netw Sci Eng, 2026, 13: 5074–5091

29 Zou K, Huang C. Cooperation dynamics on hypergraphs with punishment and Q-learning. Expert Syst Appl, 2026, 296: 128989

30 Sadekar O, Civilini A, Latora V, et al. Drivers of cooperation in social dilemmas on higher-order networks. J R Soc Interface, 2025, 22: 20250134

31 Burgio G, Matamalas J T, Gómez S, et al. Evolution of cooperation in the presence of higher-order interactions: from networks to hypergraphs. Entropy, 2020, 22: 744

32 Kumar A, Chowdhary S, Capraro V, et al. Evolution of honesty in higher-order social networks. Phys Rev E, 2021, 104: 054308

33 Zou K, Han W, Zhang L, et al. The spatial public goods game on hypergraphs with heterogeneous investment. Appl Math Comput, 2024, 466: 128450

34 Xie M, He S, Li A, et al. Transformability of dynamics on higher-order networks. Commun Phys, 2026, 9: 149

35 Xu Y, Zhao D, Chen J, et al. The nested structures of higher-order interactions promote the cooperation in complex social networks. Chaos Soliton Fract, 2024, 185: 115174

36 Wang J, Nie J, Guo S, et al. Mixing prisoner's dilemma games on higher-order networks. Neurocomputing, 2024, 607: 128439

37 Zhang Y, Lucas M, Battiston F. Higher-order interactions shape collective dynamics differently in hypergraphs and simplicial complexes. Nat Commun, 2023, 14: 1605

38 Malizia F, Corso A, Gambuzza L V, et al. Reconstructing higher-order interactions in coupled dynamical systems. Nat Commun, 2024, 15: 5184

39 Dai X, Kovalenko K, Molodyk M, et al. D-dimensional oscillators in simplicial structures: odd and even dimensions display different synchronization scenarios. Chaos Soliton Fract, 2021, 146: 110888

40 Chen J, Zou K, Zhang L, et al. Cooperation dynamics on higher-order networks: a brief review. Europhys Lett, 2025, 151: 41001

41 Battiston F, Capraro V, Karimi F, et al. Higher-order interactions shape collective human behaviour. Nat Hum Behav, 2025, 9: 2441–2457

42 Alvarez-Rodriguez U, Battiston F, de Arruda G F, et al. Evolutionary dynamics of higher-order interactions in social networks. Nat Hum Behav, 2021, 5: 586–595

43 Guo H, Jia D, Sendiña-Nadal I, et al. Evolutionary games on simplicial complexes. Chaos Soliton Fract, 2021, 150: 111103

44 Civilini A, Sadekar O, Battiston F, et al. Explosive cooperation in social dilemmas on higher-order networks. Phys Rev Lett, 2024, 132: 167401

45 Sheng A, Su Q, Wang L, et al. Strategy evolution on higher-order networks. Nat Comput Sci, 2024, 4: 274–284

46 Wang D, Yi P. Higher-order strategy evolution of cooperation on arbitrary hypergraphs. In: Proceedings of the 2025 American Control Conference, 2025. 4141–4147

47 Wang X, Zhou L, McAvoy A, et al. Strategy evolution on temporal hypergraphs. Proc Natl Acad Sci USA, 2026, 123: e2516380123

48 Xu Y, Wang J, Chen J, et al. Reinforcement learning and collective cooperation on higher-order networks. Knowl-Based Syst, 2024, 301: 112326

49 Xu Y, Zhao D, Benko T P, et al. Reinforcement learning can be a double-edged sword for cooperation on higher-order networks. IEEE Trans Syst Man Cybern Syst, 2026, 56: 231–244

50 Zou K, Huang C. Incorporating reputation into reinforcement learning can promote cooperation on hypergraphs. Chaos Soliton Fract, 2024, 186: 115203

51 Guo S, Wang J, Zhao D, et al. Role of second-order reputation evaluation in the multi-player snowdrift game on scale-free simplicial complexes. Chaos Soliton Fract, 2023, 172: 113539

52 Lin B, Zhou L, Gao Z, et al. Evolutionary dynamics of group cooperation on heterogeneous higher-order networks. IEEE Trans Netw Sci Eng, 2025, 12: 4894–4905

53 Wang D, Yi P, Hong Y, et al. Emergence of cooperation promoted by higher-order strategy updates. PLoS Comput Biol, 2025, 21: e1012891

54 Civilini A, Anbarci N, Latora V. Evolutionary game model of group choice dilemmas on hypergraphs. Phys Rev Lett, 2021, 127: 268301

55 Shen C, Song Z, Shi L, et al. Exit options sustain altruistic punishment and decrease the second-order free-riders, but it is not a panacea. Sci China Inf Sci, 2025, 68: 112204

56 Chai Y Y, Wu Z Y, Wu Y H, et al. Optimal tax-subsidy incentive for population games based on mean field approximation. Sci China Inf Sci, 2025, 68: 210213

57 Boyd R, Mathew S. A narrow road to cooperation. Science, 2007, 316: 1858–1859

58 Zhou L, Li A, Wang L. Coevolution of nonlinear group interactions and strategies in well-mixed and structured populations. J Theor Biol, 2018, 440: 32–41

59 Peña J, Nöldeke G, Lehmann L. Evolutionary dynamics of collective action in spatially structured populations. J Theor Biol, 2015, 382: 122–136

60 Archetti M, Scheuring I. Review: game theory of public goods in one-shot social dilemmas without assortment. J Theor Biol, 2012, 299: 9–20

61 Hauert C, Michor F, Nowak M A, et al. Synergy and discounting of cooperation in social dilemmas. J Theor Biol, 2006, 239: 195–202

62 Zhu W, Wang X, Wang C, et al. Evolutionary dynamics in stochastic nonlinear public goods games. Commun Phys, 2024, 7: 377

63 Jiang Y, Wang X, Zhu W, et al. Nonlinear public goods game in dynamical environments. Appl Math Model, 2026, 157: 116857

64 Zheng D F, Yin H P, Chan C H, et al. Cooperative behavior in a model of evolutionary snowdrift games with N-person interactions. Europhys Lett, 2007, 80: 18002

65 Hu M, Chen W, Yang M, et al. Evolution of cooperation based on synergy and discounting on N-person snowdrift game. In: Proceedings of the 41st Chinese Control Conference (CCC), 2022. 6922–6926

66 Gore J, Youk H, van Oudenaarden A. Snowdrift game dynamics and facultative cheating in yeast. Nature, 2009, 459: 253–256

67 Xu Y, Feng M, Zhu Y, et al. Multi-player snowdrift game on scale-free simplicial complexes. Physica A, 2022, 604: 127698

68 Kovalenko K, Sendiña-Nadal I, Khalil N, et al. Growing scale-free simplices. Commun Phys, 2021, 4: 43

69 Bianconi G, Rahmede C. Network geometry with flavor: from complexity to quantum geometry. Phys Rev E, 2016, 93: 032315

70 Chiong R, Kirley M. Effects of iterated interactions in multiplayer spatial evolutionary games. IEEE Trans Evol Comput, 2012, 16: 537–555

71 Fu F, Wang L, Nowak M A, et al. Evolutionary dynamics on graphs: efficient method for weak selection. Phys Rev E, 2009, 79: 046707

72 Benson A R, Abebe R, Schaub M T, et al. Simplicial closure and higher-order link prediction. Proc Natl Acad Sci USA, 2018, 115: E11221

73 Vanhems P, Barrat A, Cattuto C, et al. Estimating potential infection transmission routes in hospital wards using wearable proximity sensors. PLoS ONE, 2013, 8: e73970

74 Stehlé J, Voirin N, Barrat A, et al. High-resolution measurements of face-to-face contact patterns in a primary school. PLoS ONE, 2011, 6: e23176

75 Gemmetto V, Barrat A, Cattuto C. Mitigation of infectious disease at school: targeted class closure vs school closure. BMC Infect Dis, 2014, 14: 695